Origin of multiferroic spiral spin order in the $R\mathrm{MnO_3}$ perovskites

Shuai Dong,[1,2,3] Rong Yu,[1,2] Seiji Yunoki,[4] J.-M. Liu,[3,5] and Elbio Dagotto[1,2]
[1]*Department of Physics and Astronomy, University of Tennessee, Knoxville, Tennessee 37996, USA*
[2]*Materials Science and Technology Division, Oak Ridge National Laboratory, Oak Ridge, Tennessee 32831, USA*
[3]*Nanjing National Laboratory of Microstructures, Nanjing University, Nanjing 210093, China*
[4]*Computational Condensed Matter Physics Laboratory, The Institute of Physical and Chemical Research (RIKEN), Wako, Saitama 351–0198, Japan*
[5]*International Center for Materials Physics, Chinese Academy of Sciences, Shenyang 110016, China*
(Received 25 September 2008; published 21 October 2008)

The origin of the spiral spin order in perovskite multiferroic manganites $R\mathrm{MnO_3}$ (R=Tb or Dy) is here investigated using a two e_g-orbital double-exchange model. Our main result is that the experimentally observed spiral phase can be stabilized by introducing a relatively weak next-nearest-neighbor superexchange coupling (~10% of the nearest-neighbor superexchange). Moreover, the Jahn-Teller lattice distortion is also shown to be essential to obtain a realistic spiral period. Supporting our conclusions, the generic phase diagram of undoped perovskite manganites is obtained using Monte Carlo simulations, showing phase transitions from the A-type antiferromagnet, to the spiral phase, and finally to the E-type antiferromagnet, with decreasing size of the R ions. These results are qualitatively explained by the enhanced relative intensity of the superexchanges.

DOI: 10.1103/PhysRevB.78.155121 PACS number(s): 75.80.+q, 64.70.Rh, 75.30.Kz, 75.47.Lx

I. INTRODUCTION

Perovskite manganites, one of the main families of strongly correlated electronic materials, have drawn much attention since the discovery of the colossal magnetoresistance in the last decade. The strong coupling between spin, charge, orbital, and lattice degrees of freedom gives rise to many competing phases in manganites, with rich physical properties. Theoretically, the physics of manganites appears to be qualitatively understood within the framework of the double-exchange (DE) model, including the superexchange (SE) between the t_{2g} spins, and the Jahn-Teller (JT) interactions.[1]

Recently, the multiferroic materials, in which the ferroelectric (FE) and magnetic orders coexist and are intimately coupled, have become a subject of much attention due to their technological relevance and fundamental science challenges.[2,3] The discovery of multiferroicity in undoped manganites with small size R (rare-earth) cations, e.g., $\mathrm{TbMnO_3}$ and $\mathrm{DyMnO_3}$, have made the family of manganites even more fascinating.[4,5] With decreasing temperature, these multiferroic materials $R\mathrm{MnO_3}$ first transform from a paramagnetic (PM) state to a collinear spin sinusoidal incommensurate state at T_N (~40–50 K), and then to a spiral spin state with a locked period at T_{lock} (~15–30 K).[6–8] T_{lock} is also the FE critical temperature (T_c), suggesting a strong magnetoelectric interaction. In the collinear spin sinusoidal incommensurate state ($T_{\mathrm{lock}}=T_c<T<T_N$) of $\mathrm{Tb_{1-x}Dy_xMnO_3}$, all spins approximately point to the b direction and their amplitudes are modulated by the Mn positions in a sinusoidal form. The wavelength of this sinusoidal modulation, which is incommensurate to the lattice spacing, changes monotonously with decreasing temperature until T_{lock} is reached. Below T_{lock}, the spins form a coplanar (b-c) spiral order, and its wavelength is nearly independent of temperature.[8]

Such a spiral spin-order (SSO) driven improper ferroelectricity is also observed experimentally in other transition-metal oxides besides undoped manganites, such as $\mathrm{Ni_3V_2O_8}$,[9] $\mathrm{CuFeO_2}$,[10] CuO,[11] and others.[12] However, the theoretical understanding of their properties is still in its early stages. For example, the origin of the FE polarization remains under much debate. Phenomenologically, the SSO breaks the spatial inversion symmetry and allows the emergence of a spontaneous polarization.[13] Microscopically, two possible mechanisms for the FE polarization were proposed: (a) a pure electronic contribution driven by the spin-orbital coupling,[14,15] and (b) a cation displacement driven by the Dzyaloshinskii-Moriya (DM) interaction.[16,17] Interestingly, both mechanisms give the same behavior: a FE polarization $\mathbf{P}\propto-\mathbf{e}_{i,j}\times(\mathbf{S}_i\times\mathbf{S}_j)$, with $\mathbf{e}_{i,j}$ being the unit vector connecting the nearest-neighbor (NN

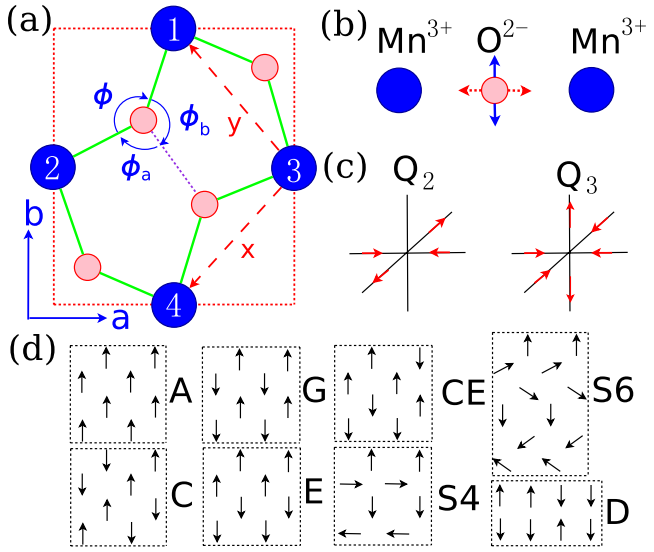

FIG. 1. (Color online) (a) Sketch of the crystal structure (*a*-*b* plane) of $R\mathrm{MnO_3}$. Two types of coordinate axes (*a*-*b* and *x*-*y*) are shown. (b) Illustration of the two kinds of distortions discussed in the text: $\mathrm{GdFeO_3}$ type (oxygen moves perpendicular to the Mn–O–Mn bond) and Jahn-Teller type (oxygen moves along Mn–O–Mn bond). (c) Two Jahn-Teller distortion modes: Q_2 and Q_3. (d) Sketch of the spin patterns (in the *a*-*b* plane) corresponding to seven (*S*4 and *S*6 belong to the same group) candidate phases considered here in the zero-temperature variational method. *A*, *G*, *CE*, *C*, and *E* are standard notations for well-known AFM phases in manganites. Here, the ferromagnetic chains in the *C*/*CE*/*E*-AFM phases are within the *a*-*b* plane. *D* denotes the $\uparrow\uparrow\downarrow\downarrow$ dimer phase that is considered in our studies although it has not been observed in real manganites (Ref. 23). In the spiral phases SL, the length period is denoted by *L* (along *x*/*y*). The $L=4$ case has the same energy as the *E*-AFM phase in the classical spin model context.

the many phases (*A*-AFM, spiral, *E*-AFM) found in $R\mathrm{MnO_3}$ manganites, since it cannot distinguish the *E*-AFM order from the $q=1/4$ spiral order (see Fig. 1) since they have the same energy. In summary, while the classical spin model with NNN magnetic frustration provides a natural starting point to describe phenomenologically the SSO phase, this simple model is not sufficient to deeply understand the microscopic origin of the SSO in perovskite manganites.

An alternative route to obtain the SSO phase is to incorporate the DM interaction ($\propto \mathbf{S}_i \times \mathbf{S}_j$) into the double-exchange framework.[16,17] However, the required intensity of the DM interaction is 2 orders of magnitude higher than expected.[16] Thus, it is fair to express that the real driving force for SSO in manganites remains a mystery. Note that a more fundamental theory to explain the origin of the SSO phase should also explain the general phase diagram of $R\mathrm{MnO_3}$: with decreasing *R* size, the ground state of $R\mathrm{MnO_3}$ changes from the *A*-type AFM (*A*) state, as in the case of $\mathrm{LaMnO_3}$, to the spiral (*S*) state, as it occurs in $\mathrm{TbMnO_3}$, and finally to the *E*-type AFM (*E*) phase, which is stabilized in $\mathrm{HoMnO_3}$. This property is referred below as the "*A*-*S*-*E* transition."[5,22] For all these phases, the order of the Mn^{3+} spins can be characterized by a particularly propagation vector $(0, q_{\mathrm{Mn}}, 1)$ (in the orthorhombic *Pbnm* cell notation, see Fig. 1), indicating an AFM coupling along the *c* axis, and FM coupling along the *a* axis. q_{Mn} is 0 for the *A* phase and 0.5 for the *E* phase. However, for convenience when using a square lattice as in our simulations, *q* in the following will be defined along the *x*/*y* directions (see Fig. 1) and it equals half of the q_{Mn} used in experimental papers.

II. MODEL AND METHODS

In this study, we will analyze the properties of the two e_g-orbital DE model for manganites defined on a two-dimensional (*a*-*b* plane) lattice to try to unveil the origin of the SSO phase in $R\mathrm{MnO_3}$. We will start from a pure DE model, and then incorporate other interactions one-by-one to clarify their respective roles. The primary Hamiltonian, considering only the DE and NN SE interactions, reads as

$$H_{\mathrm{DE+SE}} = -\sum_{\langle ij\rangle}^{\alpha\beta} t_{\mathbf{r}}^{\alpha\beta}\Omega_{ij}c_{i\alpha}^{\dagger}c_{j\beta} + J_{\mathrm{AF}}\sum_{\langle ij\rangle}\mathbf{S}_i\cdot\mathbf{S}_j, \qquad (1)$$

where the first term is the standard DE kinetic energy of the e_g electrons. The DE hopping amplitudes $t_{\mathbf{r}}^{\alpha\beta}$ are orbital and direction dependent. In particular, $t_x^{1,1}=t_y^{1,1}=3t_x^{2,2}=3t_y^{2,2}=\frac{3}{4}t_0$, $t_y^{1,2}=t_y^{2,1}=-t_x^{1,2}=-t_x^{2,1}=\frac{\sqrt{3}}{4}t_0$ where the superscript 1 (2) denotes the e_g orbital $d_{x^2-y^2}$ ($d_{3z^2-r^2}$), and t_0 (0.2–0.3 eV) is taken as the energy unit.[1] The infinite Hund coupling used here generates a Berry phase $\Omega_{ij}=\cos(\theta_i/2)\cos(\theta_j/2)+\sin(\theta_i/2)\sin(\theta_j/2)\exp[-i(\varphi_i-\varphi_j)]$, where θ and φ are the angles defining the t_{2g} spins $\mathbf{S}$ in spherical coordinates. The e_g kinetic (DE) energy is obtained by exactly diagonalizing the fermionic sector, using library subroutines, once a t_{2g} classical spins configuration is generated. The second term in the Hamiltonian is the usual AFM SE coupling between NN t_{2g} spins.

The numerical methods used in this manuscript are of two varieties: the variational method employed at zero temperature and the Monte Carlo (MC) simulation at finite temperature. For the case of the zero-temperature variational method, the total energies (per site) of several candidate phases (for an infinite size lattice) are calculated to determine which is the most likely ground state. The candidate phases are sketched in Fig. 1, and almost all of the typical spin order patterns discussed in manganites have been included. In addition, spirals with wave vectors *q* (from 0 to 1/4) are also taken into account. For the MC simulation, the classical t_{2g} spins evolve in MC time following the standard Metropolis algorithm. The MC simulation is independent of the zero-temperature variational method, namely the spin order obtained via MC simulations can be one of the candidate phases, but the outcome is unbiased and it is not limited to be one of those phases. Due to the restriction of working on a finite lattice size, a large enough cluster should be used in the MC simulation to allow for other possible spin orders. Since the MC method used here has been discussed extensively in the manganite literature, for more details regarding the Hamiltonian and the MC technique the readers are referred to Ref. 1.

III. ZERO-TEMPERATURE RESULTS

For the model studied here, the e_g electronic density is always 1 when the chemical potential equals 0. Thus, in the "clean limit" two-orbital DE model without quenched disorder, the undoped $R\mathrm{MnO_3}$ case is free from electronic phase separation tendencies, which usually occurs in doped cases.[1] Therefore, it is reasonable to consider only homogeneous phases as candidates for the ground states. A very important result in this context is that using Eq. (1) we have observed that the total energy of the spiral phase is always *higher* than the energy of both the A and the E phases, regardless of the value of J_{AF}. In other words, the spiral phase cannot be the ground state of Eq. (1), in agreement with previous studies of undoped manganites.[24] This model has to be modified for the spiral state to become the ground state in some range of parameters.

A. Role of the NNN superexchange

In the rest of the paper, the spin frustrating effects of the NNN J_2 coupling will be taken into consideration to solve this paradox. Here, J_2 arises from the superexchange between NNN $3d$ spins. It should be noted that our model is conceptually different from those based on classical spins presented in previous publications.[3,21] First, our NN SE is antiferromagnetic while it was ferromagnetic in those previous efforts. Ferromagnetic tendencies do exist in our model but they originate in the DE mechanism of itinerant e_g electrons. Second, as shown in Fig. 1, considering the substantial distance between the NNN spins via the zigzag exchange path Mn-O-O-Mn, then J_2 should be weaker than J_{AF}, in contrast to the robust J_2 used before.[3,21] As indicated in Fig. 1, the $\mathrm{GdFeO_3}$-type distortion of the oxygen octahedra, which reduces the NN Mn–O–Mn angle ϕ, is crucial for J_2, because it shortens the distance between two oxygens and increases the Mn-O-O-Mn angles. Therefore, J_2 is enhanced by the $\mathrm{GdFeO_3}$-type distortion.[21] Another important property of J_2 is its anisotropy due to $b > a$. For a crude estimation, if all $\mathrm{Mn^{3+}}$ and $\mathrm{O^{2-}}$ in Fig. 1 are simplified to be coplanar, it is easy to calculate the bond angles ϕ_b and ϕ_a from the experimental data available for a, b, and ϕ. For the case of $\mathrm{TbMnO_3}$, it was found that $b/a \approx 1.1$ and $\phi \approx 145.3°$ suggesting $\phi_b \approx 115.2$ and $\phi_a \approx 99.5°$.[5,6] The larger bond angle leads to a stronger NNN spin coupling through the Mn(1)-O-O-Mn(4) exchange path. Considering the angle dependence of the superexchange,[25] the NNN SE J_{2b} coupling between Mn(1) and Mn(4) can be between 1.8 to 2.2 times the value of the J_{2a} coupling between Mn(2) and Mn(3). In addition, the e_g orbital order can also induce this anisotropy.[21] Thus, the new term in the Hamiltonian incorporating the NNN SE coupling is

$$H_{J_2} = \sum_{[ij]} J_{2\gamma} \mathbf{S}_i \cdot \mathbf{S}_j, \tag{2}$$

where γ runs over a and b, and $[ij]$ denotes NNN sites. Considering together Eqs. (1) and (2), a zero-temperature phase diagram can be obtained by comparing the total energies of the candidate phases discussed in Fig. 1(d). As shown in Fig. 2(a), it is remarkable that now the spiral phase becomes the ground state for values of J_{2b} as small as 0.017.

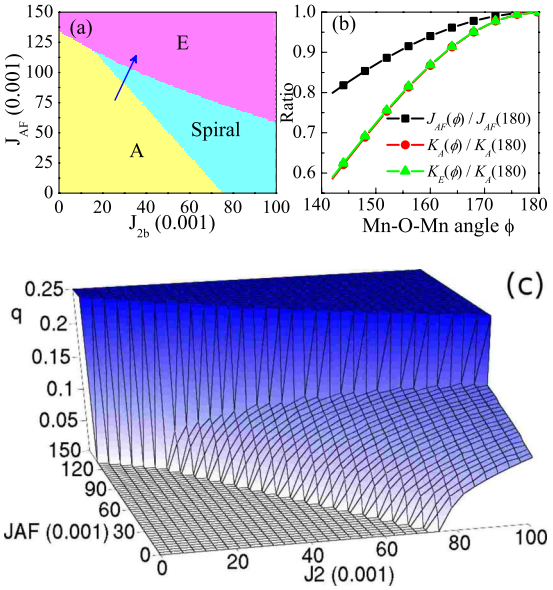

FIG. 2. (Color online) (a) Zero-temperature phase diagram of the two-orbital DE model for $R\mathrm{MnO_3}$. The possible path for the A-S-E phase transition is indicated by the arrow. The phase diagram is independent of J_{2a}, as long as $J_{2a} < J_{2b}$. (b) J_{AF}, K_{A}, and K_{E}, as a function of the Mn–O–Mn angle, normalized to their values at $\phi = 180°$. (c) Wave vector number q for (a). Here, q is defined along the x/y direction and equals half of the q_{Mn} used in experimental papers.

Considering the $\mathrm{GdFeO_3}$-type distortion, we calculated the ϕ-dependent J_{AF} (using the relation $J_{\mathrm{AF}} \propto \sin^4(\phi/2)$ described in Ref. 25) and also the DE kinetic energy (using $t^{1,1} \propto \cos^3 \phi$, $t^{1,2}$ and $t^{2,1} \propto \cos^2 \phi$, and $t^{2,2} \propto \cos \phi$, as in Ref. 26) of the A and E phases. The latter are denoted by K_A and K_E, respectively, and are shown in Fig. 2(b). Both the DE kinetic energy and J_{AF} decrease with decreasing ϕ. The curves for K_A and K_E are almost identical and lower than the J_{AF} curve. Therefore, the $\mathrm{GdFeO_3}$-type distortion increases J_{AF} relative to the DE kinetic energy. Noting that J_2 is enhanced by the $\mathrm{GdFeO_3}$-type distortion, then the total effect of this distortion is the enhancement of both the NN and NNN SE couplings, particularly the latter. Therefore, the A-S-E phase transition with decreasing R size can now be easily understood, and the arrow in Fig. 2(a) indicates a possible path that is qualitatively in agreement with experiments. Below, we will still use the ideal case $\phi = 180°$, as in most previous studies, since the $\mathrm{GdFeO_3}$-type distortion effect can be accounted for by increasing the relative values of J_{AF}/t_0 and J_2/t_0 [see Fig. 2(b)].

As shown in Fig. 2(c), at the A to S transition the wave vector q changes continuously from 0 to a finite value. However, between the spiral and E phases, not only q now changes discontinuously, but also their spin patterns are incompatible, namely the E phase is not a special case of the spiral phase. These two different phase boundaries may cause two distinct behaviors when R cations substitutions occur: (a) if Tb is substituted by an A-phase R (e.g., Gd), q will be reduced continuously; (b) if Dy is substituted by an E-phase R (e.g., Ho), phase separation at some concentrations may be induced.

B. Role of the Jahn-Teller couplings

In spite of the success in describing the SSO phase in the previous section, we have observed that in Fig. 2(c) the wave vector q is still smaller than the experimental value. For example, to obtain the q for $TbMnO_3$ (0.14 along the x/y direction), the minimum J_{2b} is 0.073 which corresponds to $J_{AF}=0.074$. This J_{2b}/J_{AF} ratio is too large for real manganites, as mentioned before in this text. Moreover, the largest q in Fig. 2 cannot reach the experimental value for $DyMnO_3$ ($q=0.19$). Even if the $GdFeO_3$-type distortion is taken into account ($\phi \approx 144.7°$ for $DyMnO_3$),[5] q cannot be increased further.

Interestingly, we have observed that realistic values for q can be stabilized if the Jahn-Teller distortion [Fig. 1(b)] is incorporated. This JT distortion can be characterized by two modes: Q_2 and Q_3 [Fig. 1(c)], which couple with the e_g electrons via

$$H_{JT} = \lambda \sum_i [Q_{2,i}\tau_{x,i} + Q_{3,i}\tau_{z,i}], \tag{3}$$

where λ is the spin-phonon coupling coefficient and τ is the orbital pseudospin operator, given by $\tau_x = c_a^\dagger c_b + c_b^\dagger c_a$ and $\tau_z = c_a^\dagger c_a - c_b^\dagger c_b$.[1] For all $RMnO_3$ at low temperatures, $|Q_2|$ and Q_3 are uniform with $|Q_2| \approx -\sqrt{3}Q_3$. The sign of Q_2 is staggered, which gives rise to the well-known staggered $d_{3x^2-r^2}$ and $d_{3y^2-r^2}$ orbital order.[25] Therefore, Eq. (3) can be scaled using $\lambda|Q_2|$ as the only parameter.

Considering together Eqs. (1)–(3), we recalculated the zero-temperature phase diagram. A typical result with $\lambda|Q_2|=1.5$ is shown in Fig. 3. Compared with Fig. 2(a), now the spiral phase region in Fig. 3(a) is enlarged. This spiral phase can even be stable without J_{2b}, although in a very narrow J_{AF} region. In Fig. 3(c), the wave vector q of the spiral phase is increased as a whole, compared with those in Fig. 2(c). Therefore, the q for $TbMnO_3$ and $DyMnO_3$ can be obtained with a small J_{2b}; e.g., the minimum J_{2b} is now 0.002 ($J_{AF}=0.091$) for $TbMnO_3$ and 0.008 ($J_{AF}=0.09$) for $DyMnO_3$, respectively. In other words, with the JT distortion incorporated, a rather weak NNN SE (<10% of NN SE) is enough to generate the realistic SSO in $RMnO_3$. In contrast to the case without JT distortions, J_{2a} also plays a prominent role here, although it cannot change the phase boundary between the *A*-*S*-*E* phases. Moreover, Fig. 3(b) shows that a robust J_{2a} even induces *C* and *D* phases in the large J_{2b} region, implying that both J_{2b} and J_{2a} in real manganites should be weak since none of these two phases have been observed experimentally in bulk $RMnO_3$.

Besides providing realistic values for q, the JT distortion can contribute to the insulating nature of $RMnO_3$, which is crucial for the FE polarization. For instance, with $\lambda|Q_2|=1.5$, the calculated gap (not shown) is 2.59 (~0.52–0.78 eV) for the spiral phase at the q of $TbMnO_3$. The agreement with experimental results for the gap (0.489 eV) suggests that the chosen value for $\lambda|Q_2|$ is reasonable.[27]

To understand the enhancement of q by the JT effect, let us focus on the *A* to *S* transition. We consider $\varphi_i=0$ and $\theta_i = 2\pi \mathbf{q}\cdot\mathbf{r}_i$ for the t_{2g} spins. After diagonalizing the fermionic operators in Eqs. (1)–(3), the ground-state energy per site is $E=K+2J_{AF}\cos(\Delta\theta)+J_{2b}\cos(2\Delta\theta)+J_{2a}$, where $\Delta\theta=2\pi q$ is the angle between NN spins, and the fermionic sector energy is $K \approx K_A \cos(\frac{\Delta\theta}{2})$. Expanding E around $\Delta\theta=0$, we obtain $E \approx E_0 - (\frac{K_A}{8} + J_{AF} + 2J_{2b})\Delta\theta^2 + (\frac{K_A}{384} + \frac{J_{AF}}{12} + \frac{2J_{2b}}{3})\Delta\theta^4 + O(\Delta\theta^6)$, where E_0 is a constant and $\Delta\theta$ (hence q) becomes an order parameter. The *A*-*S* phase boundary is determined by $\frac{K_A}{8} + J_{AF} + 2J_{2b} = 0$, which agrees with the numerical results shown in Figs. 2(a), 3(a), and 3(b). From these considerations, it is clear that the competition between K_A, J_{AF}, and J_{2b} is crucial to obtain the spiral phase using realistic interactions, distinguishing our model from the previously used effective J_1-J_2 spin models. Furthermore, the reduction of $-K_A$ by the JT distortion lowers the threshold of (J_{AF}, J_{2b}) for a spiral phase which, as a consequence, leads to an enhancement of q.

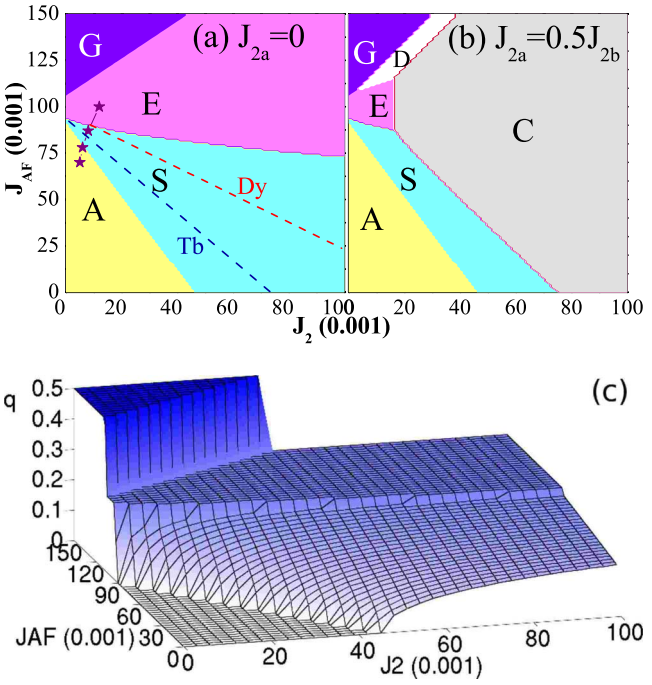

FIG. 3. (Color online) (a) Zero-temperature phase diagram of the two-orbital DE model with JT distortions ($\lambda|Q_2|=1.5$) for $RMnO_3$. The possible values of J_{AF}-J_{2b} for realistic qs in $TbMnO_3$ and $DyMnO_3$ are shown with dashed lines. The four asterisks represent the set of couplings (first and second for *A*, third for *S*, and fourth for *E*) that are studied via the MC techniques. (b) Same as (a) except for a finite $J_{2a}=0.5J_{2b}$. The four asterisks in (a) remain within the *A*-*S*-*E* region here. (c) Wave vector number q for (a).

IV. FINITE TEMPERATURE RESULTS

The above described phase diagrams were obtained at zero-temperature comparing the energies of several candidate phases. In principle, this procedure cannot rule out the possibility of other unknown phases becoming stable. Therefore, it is necessary to check the results using MC techniques. For simplicity, the spins are restricted to be in an easy plane for the magnetic moments, namely we use the XY model instead of the Heisenberg model for the t_{2g} spins. This

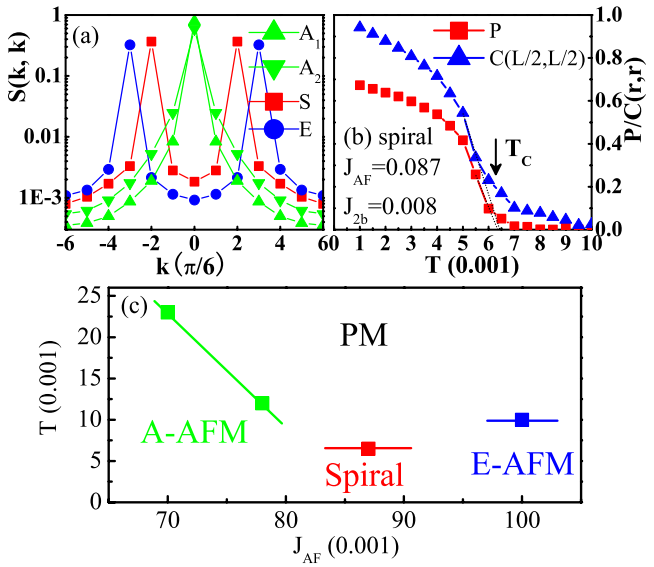

FIG. 4. (Color online) (a) Spin structure factor of the four MC simulations at $T=0.004$, corresponding to the four sets of couplings described in the text. All characteristic peaks are prominent, suggesting stable spin orders. (b) Temperature-dependent polarization P and $C(\frac{L}{2},\frac{L}{2})$ corresponding to the spiral phase with $q=1/6$. All values are normalized to their saturation values. (c) Sketch of the finite-temperature phase diagram. The T_N's for the A and E phases are determined from their $C(\frac{L}{2},\frac{L}{2})$-temperature curves. The lines connecting T_N (T_c) are just to guide the eyes.

simplification, which avoids the introduction of extra adjustable parameters to generate a magnetic anisotropy, is reasonable from the point of view of the physics of these materials since all spins are coplanar for all known low-temperature phases in $R\mathrm{MnO}_3$. The JT distortions are fixed as in the previously described zero-temperature case. **P** is obtained using the model-free equation $-\mathbf{e}_{i,j}\times(\mathbf{S}_i\times\mathbf{S}_j)$. We use a two-dimensional (2D) $L\times L$ ($L=12$) lattice with periodic boundary conditions and this computational study is carried out only at four sets of couplings (J_{2b}, J_{AF}), which are denoted by asterisks in Fig. 3(a). The very time consuming MC runs were typically carried out with 6000 steps for thermalization and 4000 steps for measurements. Considering that all the physics of the four coupling sets (asterisks) is not much affected by a weak J_{2a} [see Figs. 3(a) and 3(b)], here J_{2a} is set to be zero for simplicity. The q for the third asterisk should be the commensurate value 1/6 (suitable for $\mathrm{Tb}_{0.41}\mathrm{Dy}_{0.59}\mathrm{MnO}_3$) to match the lattice size.[8]

For all four pairs of couplings, the presence of sharp characteristic peaks in the spin structure factor of our MC results [Fig. 4(a)] confirms the stability of the candidate phases at low temperature. In addition, Fig. 4(b) shows that the T_c for the FE transition in the spiral phase is found to be 0.0065 ($\sim$16–24 K), agreeing with the experimental value 22 K.[8] It should be noted that although the Mermin-Wagner theorem forbids a finite T_c (for an infinite lattice size) in the 2D XY model, extensive MC studies on double-exchange models in the past decade have suggested that the characteristic T^* in 2D small size lattices where the order develops (namely when the correlation length becomes comparable to the lattice size) can still be comparable with the experimental critical temperatures, at least qualitatively. In a 2D regime of very large correlation lengths, a weak coupling in the third direction rapidly establishes long-range order with T^* as the critical temperature. The real-space correlation between spins at the maximum distance in our lattice $C(\frac{L}{2},\frac{L}{2})$ can also be used to provide estimations of the critical transition temperature.

Based on these considerations, here a finite-temperature phase diagram is sketched [Fig. 4(c)], guided by the four coupling sets of Fig. 3(a). It should be noted that in principle the collinear spin sinusoidal incommensurate state at $T_c<T<T_N$ is not possible in our study, because in our model the spin amplitude $|\mathrm{S}|$ is a constant and the period of the phases should be commensurate with L. Despite this finite-size effect problem, our phase diagram nevertheless resembles at least qualitatively the real one, and moreover our rough estimations for the T_N of the A and E phases also agree well with experimental results.[5]

V. CONCLUSION

In conclusion, here we have provided a microscopic description of multiferroic $R\mathrm{MnO}_3$ perovskites that explains the existence of the spiral spin-order in these compounds. The experimentally observed SSO and FE transition can be obtained by incorporating a weak NNN superexchange interaction and a Jahn-Teller distortion into the standard two-orbital DE model for manganites. Several aspects of the experimentally known A-S-E phase transition with decreasing R size are well reproduced by including the GdFeO_3-type distortion in our study. Note that this weak NNN SE interaction ($<10\%$ NN superexchange), while shown here to be crucial in the context of the manganite multiferroics, does not alter the previous large body of investigations and conclusions reached via similar MC simulations for undoped and doped LaMnO_3, since in that case the extra NNN SE couplings can be neglected.

ACKNOWLEDGMENTS

We thank N. Furukawa and K. Yamauchi for helpful discussions, and T. Kimura, S. Ishihara, and T. Hotta for useful comments. This work was supported by the NSF (Grant No. DMR-0706020) and the Division of Materials Science and Engineering, U.S. DOE, under contract with UT-Battelle, LLC. S.D. and J.M.L. were supported by the National Key Projects for Basic Research of China (Grants No. 2006CB921802 and No. 2009CB929501) and National Natural Science Foundation of China (Grant No. 50832002). S.D. was also supported by the China Scholarship Council and the Scientific Research Foundation of Graduate School of Nanjing University.

[1] E. Dagotto, T. Hotta, and A. Moreo, Phys. Rep. **344**, 1 (2001); see, also E. Dagotto, *Nanoscale Phase Separation and Colossal Magnetoresistance* (Springer, Berlin, 2002).
[2] W. Eerenstein, N. D. Mathur, and J. F. Scott, Nature (London) **442**, 759 (2006).
[3] S.-W. Cheong and M. Mostovoy, Nature Mater. **6**, 13 (2007).
[4] T. Kimura, T. Goto, H. Shintani, K. Ishizaka, T. Arima, and Y. Tokura, Nature (London) **426**, 55 (2003).
[5] T. Goto, T. Kimura, G. Lawes, A. P. Ramirez, and Y. Tokura, Phys. Rev. Lett. **92**, 257201 (2004).
[6] M. Kenzelmann, A. B. Harris, S. Jonas, C. Broholm, J. Schefer, S. B. Kim, C. L. Zhang, S.-W. Cheong, O. P. Vajk, and J. W. Lynn, Phys. Rev. Lett. **95**, 087206 (2005).
[7] T. Kimura, G. Lawes, T. Goto, Y. Tokura, and A. P. Ramirez, Phys. Rev. B **71**, 224425 (2005).
[8] T. Arima, A. Tokunaga, T. Goto, H. Kimura, Y. Noda, and Y. Tokura, Phys. Rev. Lett. **96**, 097202 (2006).
[9] G. Lawes, A. B. Harris, T. Kimura, N. Rogado, R. J. Cava, A. Aharony, O. Entin-Wohlman, T. Yildrim, M. Kenzelmann, C. Broholm, and A. P. Ramirez, Phys. Rev. Lett. **95**, 087205 (2005).
[10] T. Kimura, J. C. Lashley, and A. P. Ramirez, Phys. Rev. B **73**, 220401(R) (2006).
[11] T. Kimura, Y. Sekio, H. Nakamura, T. Siegrist, and A. P. Ramirez, Nature Mater. **7**, 291 (2008).
[12] For more details of these spiral spin multiferroics, see T. Kimura, Annu. Rev. Mater. Res. **37**, 387 (2007).
[13] M. Mostovoy, Phys. Rev. Lett. **96**, 067601 (2006).
[14] H. Katsura, N. Nagaosa, and A. V. Balatsky, Phys. Rev. Lett. **95**, 057205 (2005).
[15] C. Jia, S. Onoda, N. Nagaosa, and J. H. Han, Phys. Rev. B **74**, 224444 (2006).
[16] I. A. Sergienko and E. Dagotto, Phys. Rev. B **73**, 094434 (2006).
[17] Q. C. Li, S. Dong, and J.-M. Liu, Phys. Rev. B **77**, 054442 (2008).
[18] C. Jia, S. Onoda, N. Nagaosa, and J. H. Han, Phys. Rev. B **76**, 144424 (2007).
[19] H. J. Xiang, S.-H. Wei, M.-H. Whangbo, and J. L. F. Da Silva, Phys. Rev. Lett. **101**, 037209 (2008).
[20] A. Malashevich and D. Vanderbilt, Phys. Rev. Lett. **101**, 037210 (2008).
[21] T. Kimura, S. Ishihara, H. Shintani, T. Arima, K. T. Takahashi, K. Ishizaka, and Y. Tokura, Phys. Rev. B **68**, 060403(R) (2003).
[22] J.-S. Zhou and J. B. Goodenough, Phys. Rev. Lett. **96**, 247202 (2006).
[23] Our "dimer" phase is the $(\pi/2,\pi)$ phase proposed in H. Aliaga, B. Normand, K. Hallberg, M. Avignon, and B. Alascio, Phys. Rev. B **64**, 024422 (2001).
[24] T. Hotta, M. Moraghebi, A. Feiguin, A. Moreo, S. Yunoki, and E. Dagotto, Phys. Rev. Lett. **90**, 247203 (2003).
[25] J.-S. Zhou and J. B. Goodenough, Phys. Rev. B **77**, 132104 (2008), The NN SE coupling is proportional to $\sin^4(\phi/2)$, thus the NNN SE can be roughly estimated to be in the range $\sin^6(\phi/2) \sim \sin^8(\phi/2)$.
[26] I. A. Sergienko, C. Şen, and E. Dagotto, Phys. Rev. Lett. **97**, 227204 (2006); S. Picozzi, K. Yamauchi, B. Sanyal, I. A. Sergienko, and E. Dagotto, *ibid.* **99**, 227201 (2007).
[27] Y. Cui, C. Wang, and B. Cao, Solid State Commun. **133**, 641 (2005).